Electroluminescence from Hybrid Conjugated Polymer−CdS:Mn/ZnS Core/Shell Nanocrystals Devices

Heesun Yang* and Paul H. Holloway

Department of Materials Science and Engineering, University of Florida, Gainesville, Florida 32611-6400

Received: March 24, 2003; In Final Form: July 9, 2003

Reverse micelle-derived CdS:Mn/ZnS core/shell nanocrystals were synthesized with a core crystal diameter of 2.3 nm and a 0.4 nm thick ZnS shell and used as an electroluminescent material. Direct current (dc) electroluminescent (EL) devices were tested having a hybrid organic/inorganic multilayer structure of ITO//PEDOT-PSS//conjugated polymer//CdS:Mn/ZnS nanocrystal//Al, where two different conjugated polymers (poly(*N*-vinylcarbazole) (PVK) and poly(*p*-phenylenevinylene) (PPV)) were used. The poly(3,4-ethylenedioxythiophene)/poly(styrenesulfonate) (PEDOT-PSS) layer was used for enhanced hole injection from the ITO electrode. Orange and green EL emission was observed from devices with PVK and PPV devices, respectively. These data mean that electron−hole recombination is confined to the CdS:Mn/ZnS nanocrystalline layer in PVK-based devices but occurs in the PPV layer in PPV-based devices. Compared to a PPV EL device without a CdS:Mn/ZnS layer, the hybrid PPV-based nanocrystalline EL device showed large current flow and considerably enhanced EL emission. This suggests that the CdS:Mn/ZnS nanocrystal layer serves as an electron transport layer (ETL) in the hybrid device. These observations are shown to be consistent with the energy level diagrams of the EL devices.

1. Introduction

Recently, electroluminescent (EL) devices using undoped or doped semiconductor nanocrystals have been investigated.[1−10] Most of the nanocrystal-based EL devices consist of a hybrid organic/inorganic structure, where either an organic conjugated polymer and inorganic nanocrystal component exist as a separate layer[3−8] or nanocrystals are embedded in a conjugated polymer matrix.[9,10] Like organic light emitting diodes (OLEDs), efficient charge injection and transport are important in hybrid nanocrystal-based EL devices. The electrons and holes injected from respective electrodes combine inside semiconductor nanocrystal and/or conjugated polymer layers, with characteristic lights being emitted as a result of the recombination of these carriers. The electron and hole current flows across the EL device are mainly determined by the energy levels of the individual component of the EL device. The location of recombination and device efficiency are controlled by the mismatch of those energy levels. In general, improved device efficiency can be accomplished by adding electron transport layers (ETL) and/or hole transport layers (HTL).[11,12] Colvin et al.[3] demonstrated that although a double layer structure having separate poly(*p*-phenylenevinylene) (PPV) (as a hole transport layer) and CdSe nanocrystal layers showed reasonable EL performance, a device with only a CdSe nanocrystal layer did not exhibit detectable EL emission. Also Yang et al.[8] reported that a poly(3,4-ethylenedioxythiophene)/poly(styrenesulfonate) (PEDOT-PSS) layer led to enhanced current flow through a ZnS:Mn nanocrystalline device because of a lower energy barrier for hole injection from the ITO electrode, as well as enhancement of the hole mobility in PEDOT-PSS.

Organically passivated nanocrystals still have a relatively large number of unpassivated surface sites.[13] These unpassivated surface sites act as nonradiative recombination and photodegradable sites, and thus suppress the efficient luminescence and promote photodegradation of the devices.[14,15] Therefore, control of the nanocrystal surface has been a critical issue to obtain highly luminescent nanocrystals and enhanced photostability. Inorganically passivated nanocrystals (or core/shell structure) such as CdSe/CdS,[14] CdSe/ZnS,[15] and ZnSe/ZnS[16] have been reported to be an improvement over those passivated by organic surface layers. Using inorganic materials with a wider band gap, surface-related defect states could be effectively passivated, leading to enhanced photostability as well as improved quantum efficiency.[14−16] Schlamp et al.[4] reported an EL device based on CdS-passivated CdSe (CdSe/CdS) nanocrystalline and PPV layers. Simultaneous EL emissions from both the PPV and CdSe/CdS nanocrystal layers in the ITO//PPV//CdSe/CdS//Mg−Ag device structure were observed, indicating that electron−hole recombination occurs in both layers.

In this study, ZnS-passivated CdS:Mn nanocrystals are synthesized for a yellow emitting nanocrystal phosphor. EL devices having a multilayer structure were constructed using conjugated polymers (PVK and PPV), and ZnS-passivated CdS:Mn nanocrystals. These nanocrystal-based EL devices exhibit a single EL emission from either the conjugated polymer or CdS:Mn/ZnS nanocrystal layer, rather than simultaneous EL emission from both layers. On the basis of the energy level diagrams of the EL devices, the different roles of the conjugated polymer and the nanocrystal layers for hole transport, electron transport, and recombination for emission are proposed.

2. Experimental Section

Synthesis of CdS:Mn/ZnS Core/shell Nanocrystals. ZnS-passivated CdS:Mn nanocrystals were prepared via a reverse micelle method. In this method, $Cd(CH_3COO)_2 \cdot 2H_2O$, $Mn(CH_3COO)_2$, Na_2S, and $Zn(CH_3COO)_2$ were used for preparation

* Corresponding author. Fax: 352 392 4911. E-mail: hyang@ufl.edu.

10.1021/jp034749i CCC: $25.00
Published on Web 08/05/2003

of (Cd^{2+} + Mn^{2+})-, S^{2-}-, and Zn^{2+}-containing standard aqueous solutions. Each aqueous solution was stirred with dioctyl sulfosuccinate, sodium salt (AOT)/heptane solution, forming the micellar solution. Mn-doped CdS core nanocrystals were formed by mixing (Cd^{2+} + Mn^{2+})- and S^{2-}-containing micellar solutions rapidly for 10−15 min. For growth of a ZnS shell layer, Zn^{2+}-containing micellar solution is added at a very slow rate (1.5−2 mL/min) into the CdS:Mn core nanocrystal micellar solution (while maintaining a surplus of S ions to support ZnS shell growth). The homogeneous nucleation and growth of any pure ZnS crystallites were suppressed by the very slow addition of the Zn^{2+} micellar solution. In this reverse micelle route, the concentrations of Cd^{2+} and Zn^{2+} ions in water are 0.1 and 0.065 M, respectively. Also the concentrations of water and AOT in heptane are 1 and 0.1 M, respectively, and the ratio of solution concentration of ZnS to CdS is four. The molar ratios of water-to-surfactant (*W)* are 10 for formation of CdS:Mn core nanocrystals and 20 for the ZnS shell layer. The Mn solution concentration in CdS is 2 mol %. For a comparison of organic versus inorganic passivation, *n*-dodecanethiol-passivated CdS:Mn nanocrystals were synthesized with the same *W* ratio and Mn concentration. After addition of the Zn^{2+} micellar solution, a small amount of methanol was added to precipitate nanocrystals, which were washed by centrifugation (9000 rpm, 8 min) more than three times with methanol and finally dispersed in methanol.

Fabrication of Hybrid Electroluminescence Devices. The hybrid EL device consisting of ITO//PEDOT-PSS//PVK//CdS:Mn/ZnS//Al was constructed as follows. The 30 nm thick PEDOT-PSS layer was spin-deposited onto the cleaned ITO-coated glass substrate. The 120 nm thick PVK layer was spin-deposited on the PEDOT-PSS layer, followed by the deposition of methanol-dispersed CdS:Mn/ZnS nanocrystals. The CdS:Mn/ZnS nanocrystal layer was dried using a vacuum oven at 60 °C and resulted in a layer 80 nm thick. The 300 nm thick Al contact, 3 mm in diameter, was vacuum-evaporated onto the nanocrystal layer to complete the device. To operate the device, positive and negative voltages were applied to the ITO and Al electrodes, respectively.

The second hybrid EL structure, where PPV conjugated polymer was used instead of PVK, had a structure of ITO//PEDOT-PSS//PPV//CdS:Mn/ZnS//Al. The 20 nm PPV layer was formed by spin-depositing water-diluted poly(xylylene tetrahydrothiophenium chloride) (precursor PPV) onto the PEDOT-PSS-deposited ITO glass substrate, and then thermally converting the precursor film into a PPV film in a vacuum oven at 160 °C for 12 h. The same procedures as above were followed to complete the EL device. In addition, an EL device without a CdS:Mn/ZnS nanocrystal layer, ITO//PEDOT-PSS//PPV//Al, was constructed for comparison.

Characterization. A JEOL 2010F transmission electron microscope (TEM) operated at 200 kV was used for imaging and direct determination of crystal size. For TEM samples, the dilute solution of nanocrystals in methanol was dropped onto a carbon-coated copper grid, dried and placed in the microscope. The film thickness was measured with a Tencor P-10 profilometer. Photoluminescence (PL) excitation and emission spectra were collected at room temperature using a monochromatized Xe light source (300 W). The EL brightness was characterized as a function of voltage across the device. EL emission was collected by a fiber optic and dispersed onto a CCD Si detector (Ocean Optics Spectrometer). The voltage was supplied by a dc power supply and a Keithley 238 ammeter was used to measure the current.

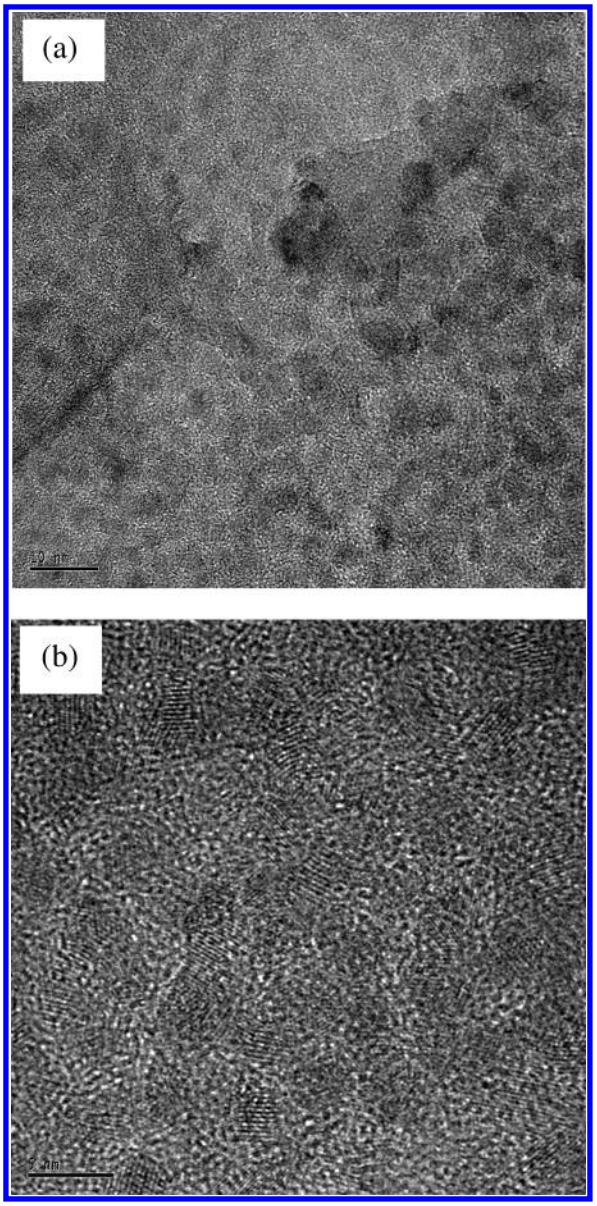

Figure 1. Transmission electron microscope (TEM) images with low (a) and high magnification (b) of CdS:Mn/ZnS nanocrystals, showing a mean particle size of 3.1 nm. The length bars at lower left corner in Figure 1a,b indicate 10 and 5 nm, respectively.

3. Results and Discussion

Size Information on Core/shell Nanocrystals. Transmission electron microscope (TEM) images of CdS:Mn/ZnS nanocrystals are shown in Figure 1. The average size of core/shell nanocrystals was observed to be 3.1 nm. The Figure 1b shows the lattice fringes of CdS:Mn/ZnS nanocrystals clearly; however, the image contrast between the CdS core and ZnS shell is not distinguishable. The nanocrystal size was also approximated by using X-ray diffraction (XRD) data and the Debye−Scherrer equation to be 2.3 nm, indicating the ZnS shell thickness of 0.4 nm. The size calculated from the XRD reflects only the CdS:Mn core, since Peng et al.[14] demonstrated that the shell layer does not affect the XRD peak width from the core in a CdSe/CdS core/shell structure.

Electroluminescence and Electrical Properties from Hybrid Conjugated Polymers-Core/shell Nanocrystals Devices. Emission spectra as a function of applied voltages from an EL device consisting of ITO//PEDOT-PSS//PVK//CdS:Mn/ZnS//Al are shown in Figure 2. The intensity of EL emission increased

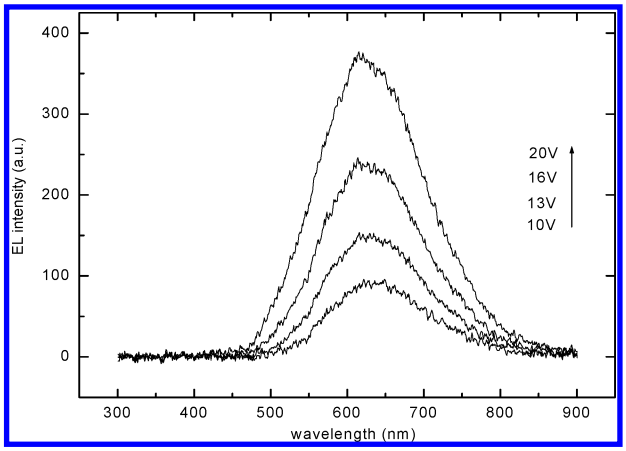

Figure 2. EL spectra from an ITO//PEDOT-PSS//PVK//CdS:Mn/ZnS// Al hybrid device as a function of applied voltages.

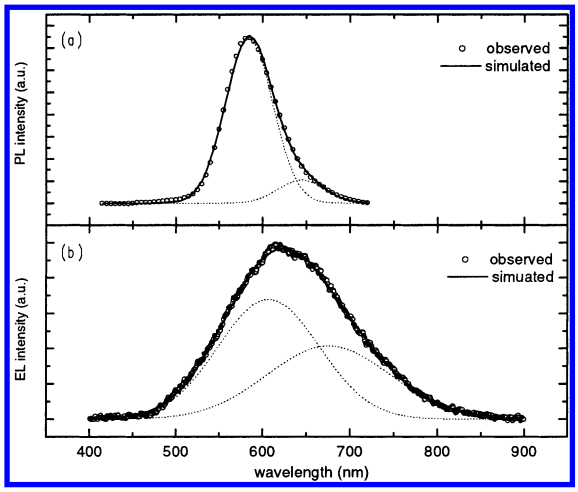

Figure 3. Peak fitting of PL emission (a) and EL emission (b) spectra by summation of two Gaussian peaks. The applied voltage for EL and excitation wavelength for PL emission are 16 V and 360 nm, respectively.

with increased applied voltage without any change in emission wavelength. In the absence of the PEDOT-PSS layer, no noticeable EL emission was observed. This is thought to result from the fact that PEDOT-PSS both lowers the energy barrier for hole injection from the ITO electrode and enhances the hole mobility.[8] PL and EL emission spectra are shown in Figure 3a,b, respectively. The PL emission is from the CdS:Mn/ZnS nanocrystal layer on the glass substrate. The PL emission peak at ∼585 nm is due to the Mn $^4T_1-^6A_1$ transition but exhibits a broad tail at longer wavelengths. The EL emission peak is at ∼620 nm, i.e., exhibits a relatively large red-shift and broad peak versus the PL peak, again with a long wavelength tail. Assuming PL and EL emission can be described with a Gaussian function, both emission envelopes can be fit by two peaks, as shown in Figure 3. The PL peak at 645 nm has been attributed to emission from internal defects, such as sulfur vacancies.[17,18] It appears reasonable that the emission peaks at 585 and 645 nm observed in PL are red-shifted to 605 and 675 nm in EL. The red-shift and broader bandwidth of EL emission relative to PL emission are well-known in nanocrystal-based EL.[2,4,7,9] Notice that the contribution from defect-related emission is more pronounced in EL than in PL. Schlamp et al.[4] proposed that the red-shift of EL emission, observed in CdSe/CdS core/shell nanocrystal-based EL devices, could be attributed to either stronger reabsorption of the short wavelength EL emission by the quantum-shifted nanocrystal layer or result from size

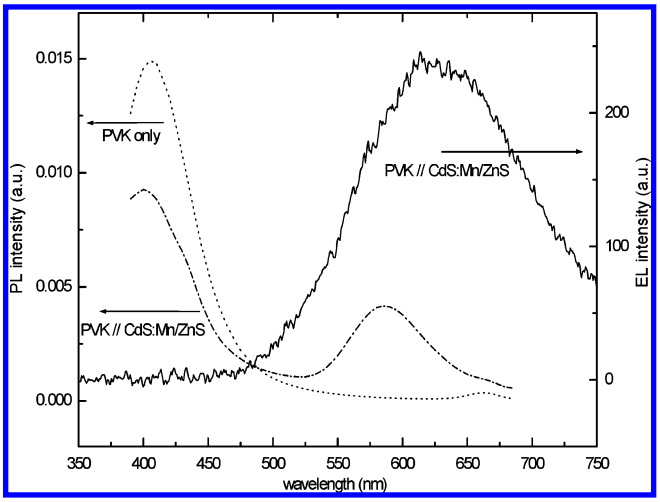

Figure 4. Comparison of PL and EL emission spectra obtained from an ITO//PEDOT-PSS//PVK//CdS:Mn/ZnS//Al device. PL emission spectrum of PVK-only is shown for comparison. The applied voltage for EL and excitation wavelength for PL emission are 16 V and 360 nm, respectively.

selection of either charge injection (larger injection barrier exists for smaller nanocrystals) or Föster energy transfer from small to large nanocrystals. Although intrinsic semiconducting materials such as nanocrystalline CdSe may exhibit such a band-edge (excitonic) transition reflecting quantum shifts of their band gap, impurity-doped semiconductors such CdS:Mn show unique impurity-related transitions. Thus, the reason for red-shift EL emission for the present material cannot be explained by these mechanisms. Rather, the red-shift as well as broader EL emission peaks relative to PL is postulated to be due to local Joule heating from the large current flux and poor thermal conductivity of the emitting layer, as reported previously.[2,9]

Recall that EL emission from PVK is not observed from a ITO//PEDOT-PSS//PVK//CdS:Mn/ZnS//Al device. Most nanocrystal-based EL devices using a conjugated polymer as a charge transport layer show emission from both the nanocrystal and polymer layers, due to electron−hole recombination in both components.[3,4,9] PL emission was collected from the same EL sample and compared with EL data (Figure 4). As a reference, PL emission from PVK layer only is also shown in Figure 4. Blue and orange PL peaks at ∼405 and ∼585 nm are observed due to PVK and CdS:Mn/ZnS nanocrystals, respectively.

The current−voltage ($I-V$) characteristic of a device consisting of ITO//PEDOT-PSS//PVK//CdS:Mn/ZnS//Al is shown in Figure 5a. EL emission was only observed under a forward bias, i.e., when a positive voltage is applied to the ITO electrode. The log I/log V plot in Figure 5b suggests an ohmic-like behavior ($I \propto V$) at low voltages (<8 V), indicating that conductance is limited by the PVK and CdS:Mn/ZnS nanocrystal layers rather than interfaces between them and/or electrode interfaces. At higher voltages (<8 V) the data follow the trapped-charge-limited-current (TCLC) model, i.e., $I \propto V^m$ with $m \approx 5$. This suggests that above 8 V, a fraction of carriers injected from the electrodes participates in current flows while the balance are immobilized by traps.[19,20] Several organic light emitting devices have been demonstrated to exhibit an $I \propto V^m$ relation with different values of m, depending on the type of organic materials and the depth of the trap (i.e., the trap energy).[20,21]

PPV is a conjugated polymer, which is widely used as emitting layer in OLEDs and as a hole transport layer in nanocrystal-based EL devices. Additional multilayer EL struc-

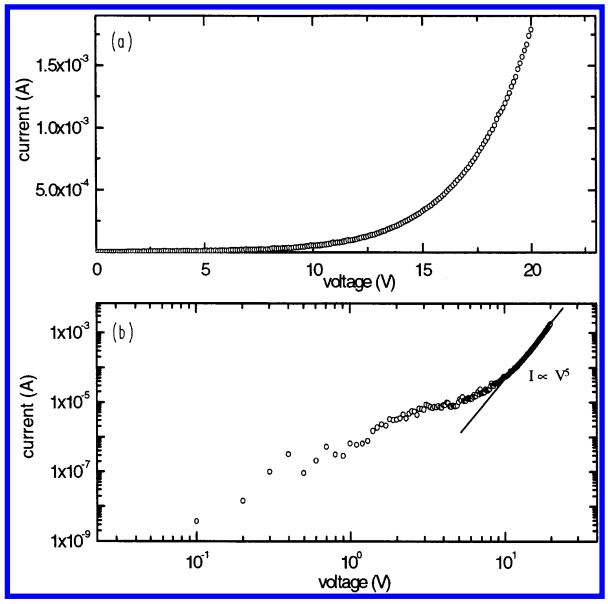

Figure 5. Current (I)−voltage (V) (a) and log I−log V characteristics (b) from an ITO//PEDOT-PSS//PVK//CdS:Mn/ZnS//Al EL device.

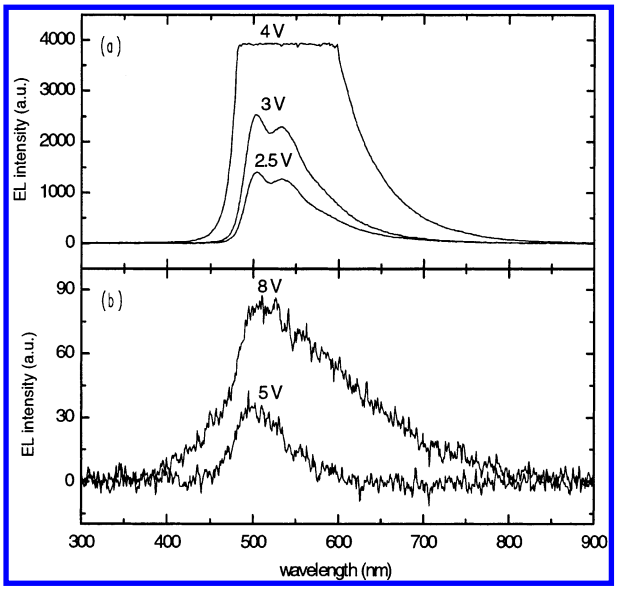

Figure 6. Comparison of EL emission spectra as a function of applied voltages from (a) ITO//PEDOT-PSS//PPV//CdS:Mn/ZnS//Al and (b) ITO//PEDOT-PSS//PPV//Al EL devices.

tures consisting of either ITO//PEDOT-PSS//PPV//CdS:Mn/ZnS//Al or ITO//PEDOT-PSS//PPV//Al were fabricated. EL emission spectra as a function of applied voltages from ITO//PEDOT-PSS//PPV//CdS:Mn/ZnS//Al and ITO//PEDOT-PSS//PPV//Al devices are shown in Figure 6a,b, respectively. In terms of EL intensity, the device with the CdS:Mn/ZnS nanocrystal layer was much brighter at the same voltage than the one with only PPV. Although a detectable EL emission requires ∼5 V in the PPV-only device, the device with the nanocrystal layer exhibits a bright EL emission even at ∼2.5 V. At 5 V, the EL emission is sufficiently intense to saturate the detection. However, the EL emission from the nanocrystal layer devices originates from only the PPV layer, not the CdS:Mn/ZnS layer or both layers (see Figure 7). This is completely different from the ITO//PEDOT-PSS//PVK//CdS:Mn/ZnS//Al devices, where EL emission results from the CdS:Mn/ZnS nanocrystal layer. The EL and PL spectra collected from ITO//PEDOT-PSS//PPV//CdS:Mn/ZnS//Al devices, and PL emission from PPV-only devices are shown in Figure 7. In PL, green and orange PL

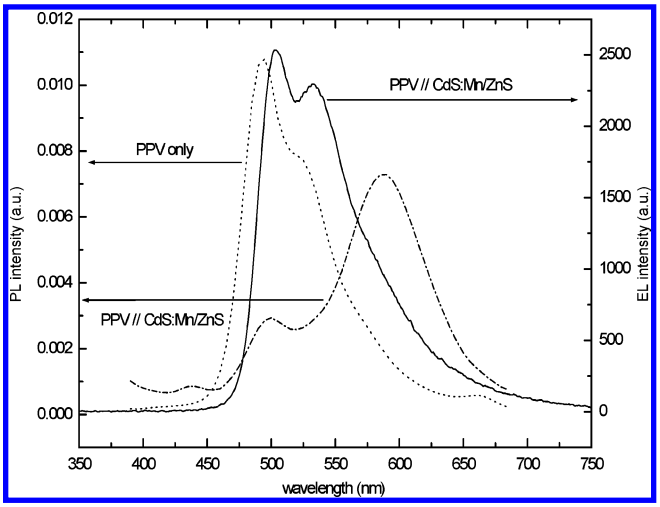

Figure 7. Comparison of PL emission and EL emission spectra obtained from ITO//PEDOT-PSS//PPV//CdS:Mn/ZnS//Al device structures. The PL emission spectrum of PPV-only is shown for comparison. The applied voltage for EL and excitation wavelength for PL emission are 3 V and 360 nm, respectively.

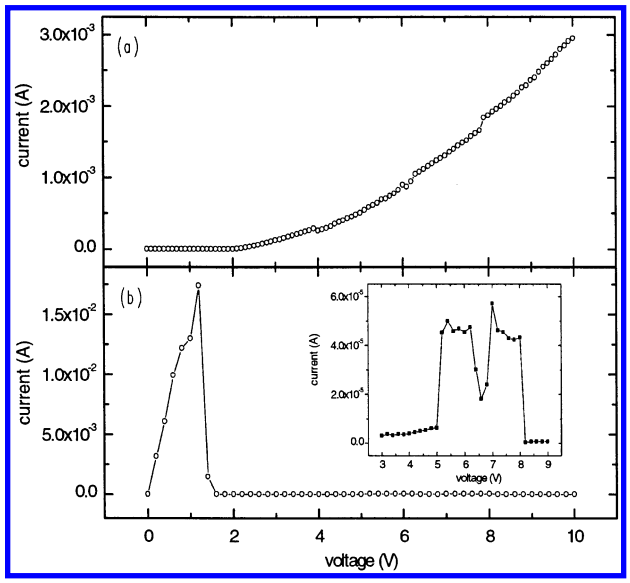

Figure 8. Comparison of I−V data from (a) ITO//PEDOT-PSS//PPV//CdS:Mn/ZnS//Al and (b) ITO//PEDOT-PSS//PPV//Al EL devices. The inset in (b) is the magnified plot between 3 and 9 V (see text).

peaks at ∼500 and ∼585 nm are observed from the PPV and CdS:Mn/ZnS nanocrystal layers, respectively. The I−V characteristics of ITO//PEDOT-PSS//PPV//CdS:Mn/ZnS//Al and ITO//PEDOT-PSS//PPV//Al devices are shown in Figure 8a,b, respectively, and the effect of the CdS:Mn/ZnS nanocrystal layer on current flow is dramatic. In the device with the CdS:Mn/ZnS nanocrystal layer, the current increased with voltage in a power law fashion. In the device with only PPV, a large leakage current flows up to an applied voltage of ∼1.5 V, but current drops to near zero at higher voltages. This leakage current does not contribute to EL emission and did not appear upon reapplying the voltage. The inset in Figure 8b shows that small current flows were observed between 3 and 9 V. This small and irregular current flow did result in weak EL emission from the ITO//PEDOT-PSS//PPV//Al device.

Proposed Energy Diagrams of Devices. The energy level diagrams of devices consisting of ITO//PEDOT-PSS//PVK//CdS:Mn/ZnS//Al and ITO//PEDOT-PSS//PPV//CdS:Mn/ZnS//Al are shown in Figure 9a,b, respectively. The work functions, band gaps, and electron affinities of ITO, Al, PEDOT-PSS,

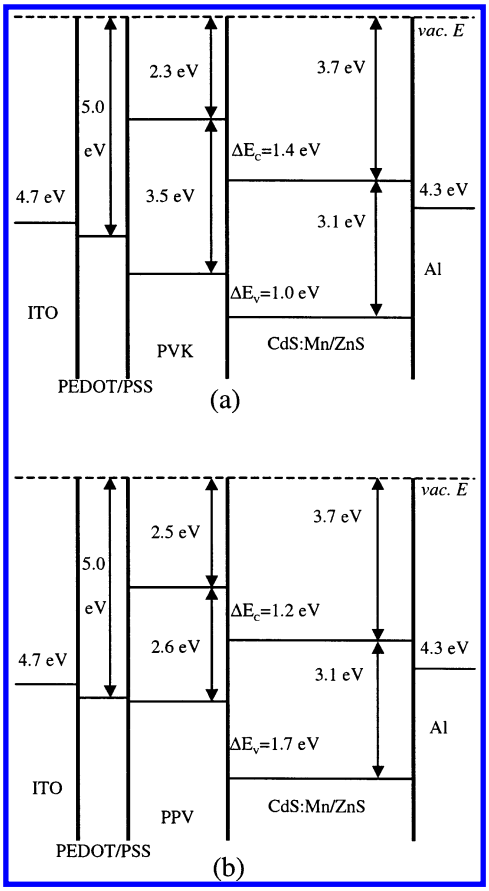

Figure 9. Proposed energy level diagrams of (a) an ITO//PEDOT-PSS//PVK//CdS:Mn/ZnS//Al device and (b) an ITO//PEDOT-PSS//PPV//CdS:Mn/ZnS//Al EL device.

PVK, and PPV are values reported in the literature. Note that because the ZnS capping layer is so thin (<1 nm), its energy levels are not shown in Figure 9. The electron affinity of the CdS in the nanocrystal layer is extrapolated from that (∼4.4 eV) of bulk CdS,[22] on the basis of the effective mass approximation (quantum confinement) theory.[22,23] Due to the lighter effective mass of electrons versus holes in CdS ($m_h/m_e \sim 4$),[22,24] the electron affinity of CdS nanocrystal depends mostly on the energy of the conduction band edge. The band gap (∼3.1 eV) of theCdS core nanocrystal is determined from UV−visible absorption data (not shown here). An EL device with neither a PVK nor a PPV layer (i.e., ITO//PEDOT-PSS//CdS:Mn/ZnS//Al) was tested but no EL emission was observed. As shown by the energy band diagrams (Figure 9), this lack of emission may be attributed to a large hole injection barrier at the PEDOT-PPS//CdS:Mn/ZnS interface. The presence of a PVK layer makes hole injection into the nanocrystal layer efficient by lowering this energy barrier. In the case of a PPV layer, the ionization potential of PPV is comparable to the work function of PEDOT-PSS and the PPV layer does not lower the energy barrier for hole injection into the nanocrystal layer. Although the energy barrier for electron injection at the CdS:Mn/ZnS//Al interface remains constant independent of the polymer layer, the energy barrier (∼0.1 eV) for hole injection at the PEDOT-PSS//PPV interface is lower than that (∼0.8 eV) at the PEDOT-PSS//PVK interface. This is consistent with the fact that the PPV-based nanocrystal devices have a lower turn-on voltage and higher current flow at the same voltage as compared to the PVK-based devices. As shown in Figures 2 and 6a, orange emission from the CdS:Mn/ZnS nanocrystal layer is dominant from PVK-based hybrid devices, whereas green emission from the PPV layer is dominant from PPV-based hybrid devices. This clearly implies that the electron−hole recombination occurs in different regions for the two different EL devices. On the basis of the energy levels shown in Figure 8, the offset of the conduction bands at the PVK//CdS:Mn/ZnS heterojunction is larger (1.4 eV) than that of the valence bands (1.0 eV); therefore, hole injection into the CdS:Mn/ZnS nanocrystal layer is favored and recombination of electron and hole in the CdS:Mn/ZnS nanocrystal layer is dominant. In contrast, for a PPV-based nanocrystal device, the PPV//CdS:Mn/ZnS conduction band offset is lower (1.2 eV) than the valence band offset (1.7 eV). These offsets would favor electron injection from CdS:Mn/ZnS nanocrystals into PPV and recombination of electron and hole in the PPV layer. The large differences in EL emission intensity and current flow of PPV-based nanocrystal and PPV-only EL devices were shown in Figures 6 and 8. Compared to PPV-only devices, PPV-based nanocrystal hybrid EL devices exhibit much greater EL brightness and larger current flows. This is presumably due to the enhanced electron injection from the nanocrystalline layer between PPV and Al. This results from the CdS:Mn/ZnS nanocrystal layer serving as an electron transport layer with high conductance, and from enhanced electron flow due to lowering of the energy barrier for electron injection.

4. Conclusions

Nanocrystals with a CdS:Mn/ZnS core/shell structure with a core crystal diameter of 2.3 nm and a shell thickness of 0.4 nm were synthesized via a reverse micelle route. Hybrid electroluminescent devices with a multilayer structure were fabricated using CdS:Mn/ZnS core/shell nanocrystals and conjugated polymers such as PVK and PPV. In PVK-based nanocrystal devices, only orange emission from the CdS:Mn/ZnS nanocrystal layer was observed, with no emission from the PVK. However, only green EL emission was observed from the PPV layer in PPV-based nanocrystal hybrid devices, with no emission from the nanocrystalline layer. EL emission from a single layer of a multilayer structure was concluded to result from radiative electron−hole recombination occurring predominantly in that layer. The current−voltage characteristic of PVK-based nanocrystal hybrid EL devices was discussed, and the trapped-charge-limited-current (TCLC) model was suggested to describe the behavior at voltages >8 V. PPV-only EL devices showed much smaller current flow and weaker EL emission than PPV-based nanocrystal hybrid EL devices. All of these data were interpreted in terms of energy levels for the PVK, PPV, and quantum-shifted CdS:Mn/ZnS structures. When the valence band offset was smaller than the conduction band offset (PVK-based hybrid device), recombination occurred in the nanocrystalline layer. When the conduction band offset was less that the valance band offset (PPV-based hybrid device), recombination occurred in the conjugated polymer.

Acknowledgment. This work was supported by ARO Grant No. DAAD19-01-1-0603.

References and Notes

(1) Aetemyev, M. V.; Sperling, V.; Woggon, U. *J. Appl. Phys*. **1997**, 81, 6975.

(2) Huang, J.; Yang, Y.; Xue, S.; Yang, B.; Liu, S.; Shen, J. *Appl. Phys. Lett*. **1997**, *70*, 2335.

(3) Colvin, V. L.; Schlamp, M. C.; Alivisatos, A. P. *Nature* **1994**, *370*, 354.

(4) Schlamp, M. C.; Peng, X.; Alivisatos, A. P. *J. Appl. Phys*. **1997**, *82*, 5837.

(5) Gao, M.; Richter, B.; Kirstein, S.; Mohwald, H. *J. Phys. Chem. B* **1998**, *102*, 4096.

(6) Mattoussi, H.; Radzilowski, L. H.; Dabbousi, B. O.; Thomas, E. L.; Bawendi, M. G.; Rubner, M. F. *J. Appl. Phys*. **1998**, *83*, 7965.

(7) Chen, W.; Grouquist, D.; Roark, J. *J. Nanosci. Nanotechnol*. **2002**, *2*, 47.

(8) Yang, H.; Holloway, P. H. *J. Appl. Phys.* **2003**, *93*, 586.

(9) Dabbousi, B. O.; Bawendi, M. G.; Onitsuka, O.; Rubner, M. F. *Appl. Phys. Lett*. **1995**, *66*, 1316.

(10) Tessler, N.; Medvedev, V.; Kazes, M.; Kan, S.; Banin, U. *Science* **2002**, *295*, 1506.

(11) Shaheen, E.; Jabbour, E.; Kippelen, B.; Grubbs, H. *Appl. Phys. Lett*. **1999**, *74*, 3212.

(12) Chkoda, L.; Heske, C.; Sokolowski, M.; Umbach, E.; Simmerer, J. *Synth. Met*. **2000**, *111*−112, 315.

(13) Wang, Y.; Herron, N. *J. Phys. Chem*. **1991**, *95*, 525.

(14) Peng, X.; Schlamp, M. C.; Kadavanich, A. V.; Alivisatos, A. P. *J. Am. Chem. Soc*. **1997**, *119*, 7019.

(15) Hines, M. A.; Guyot-Sionnest, P. *J. Phys. Chem*. **1996**, *100*, 468.

(16) Song, K.; Lee, S. *Current Appl. Phys*. **2001**, *1*, 169.

(17) Levy, L.; Ingert, D.; Feltin, N.; Pileni, M. P. *J. Cryst. Growth* **1998**, *184*−*185*, 377.

(18) Sun, L.; Fu, X.; Wang, M.; Liu, C.; Liao, C.; Yan, C. *J. Lumin*. **2000**, *87*−*89*, 538.

(19) Chayet, H.; Faraggi, E. Z.; Hong, H.; Savvate'ev, V. N.; Neumann, R.; Avny, Y.; Davidov, D. *Synth. Met*. **1997**, *84*, 621.

(20) Burrows, R. E.; Shen, Z.; Bulovic, V.; McCarty, D. M.; Forrest, S. R. *J. Appl. Phys*. **1996**, *79*, 7991.

(21) Jeong, H.; Lee, Y.; Talaie, A.; Kim, K.; Kwon, Y.; Jang, J. *Thin Solid Films* **2002**, *417*, 171.

(22) Brus, L. E. *J. Chem. Phys*. **1983**, *79*, 5566.

(23) Brus, L. E. *J. Chem. Phys*. **1984**, *80*, 4403.

(24) Sze, S. M. *Physics of Semiconductor Devices*, 2nd ed.; John Wiley & Sons: 1981; p 849.